J. Fluid Mech. (1978), *vol.* 85, *part* 4, *pp.* 787–794
Printed in Great Britain

Wilson Cloud formation by low-altitude nuclear explosions

By R. E. WALTZ
Visidyne, Inc., Burlington, Massachusetts 01803†

(Received 23 May 1977)

A model of Wilson Cloud formation following a low-altitude nuclear detonation is developed. It is shown that, for detonation yields between 10^{-3} kt and 100 kt, simple scaling laws characterize the evolution and physical properties of the Wilson Cloud.

1. Introduction

In this article we shall deal with the Wilson Cloud formed by low-altitude nuclear explosions as described in Glasstone (1962). Despite the fact that this is a well-known phenomenon, we have found no detailed treatment of it in the literature. The basis of the effect is straightforward. During the weak shock phase of an explosion, the pressure behind the shock front becomes less than the ambient atmospheric pressure over a certain volume. Thus parcels of air passing through the shock undergo a rapid expansion which can temporarily drive the relative humidity to supersaturation. Under these conditions, the radii of water-droplet aerosols present can grow by many orders of magnitude, thereby momentarily forming a cloud in a region behind the advancing shock. We shall restrict the discussion here to maritime aerosols composed of salt-solution droplets.

We shall demonstrate (i) that there is a threshold of ambient relative humidity for significant cloud formation independent of the explosion energy and (ii) that over a wide range of explosion energies the maximum cloud droplet sizes are nearly independent of the ambient aerosol spectrum and may be scaled with the explosion energy.

In § 2, we discuss the hydrodynamic flow behind the shock wave and its effect on the relative humidity which drives the cloud formation. In § 3, we review droplet growth kinetics and the basis for droplet size scaling. Finally, we give in § 4 a universal scaled formulation of the droplet size and cloud location together with a discussion of the limitations on our approach.

2. Shock humidity profiles

We shall concern ourselves here with the time t, the history of the relative humidity S and the temperature T (°K) of an air parcel passing through the shock wave. The parcel will be denoted by its initial altitude z and its radial distance r from the explosion centre. S is given by

$$S \equiv [X/(X+\epsilon)]\, P/\bar{p}, \tag{2.1}$$

where P is the pressure, X is the vapour mixing ratio (grams of water vapour per gram of dry air), ϵ is the molecular weight of water vapour relative to that of air (0·621) and

† Present address: General Atomic Company, San Diego, California 92138.

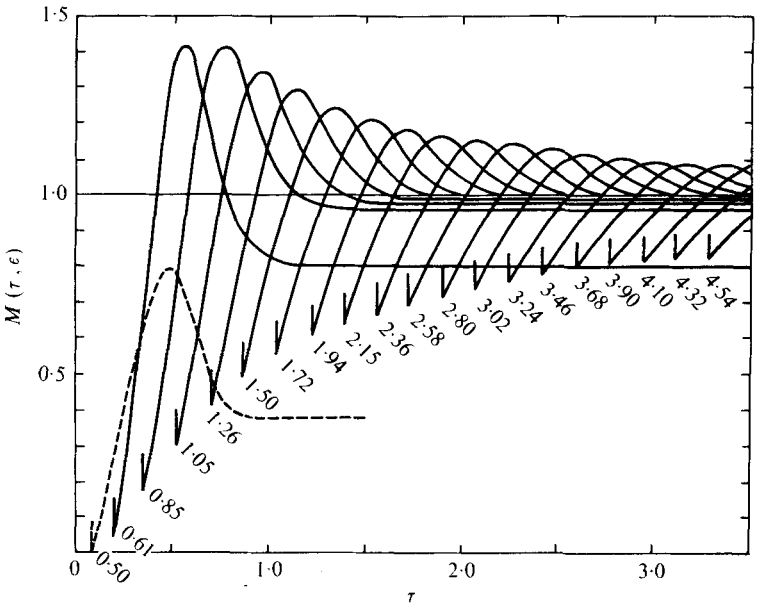

FIGURE 1. Universal shocked relative humidity multiplying function M *vs.* dynamic time τ for air parcels at various dynamic lengths l (curve labels).

$\bar{p}(T)$ is the saturation vapour pressure:

$$\bar{p}(T) \equiv (3{\cdot}53 \times 10^4 \,\text{dyne cm}^{-2}) \exp\left[-(L\epsilon/R_d)(1/T - \tfrac{1}{300})\right], \tag{2.2}$$

where L is the heat of vaporization of water ($2{\cdot}42 \times 10^{10}\,\text{erg g}^{-1}$) and R_d is the dry-air gas constant ($2{\cdot}87 \times 10^6\,\text{erg g}^{-1}\,^\circ\text{K}^{-1}$).

A crucial simplifying assumption results from neglecting the water condensation ΔX compared with X. Existing dry-air calculations of shock wave profiles for pressure and temperature assume that the flow behind the shock wave is adiabatic, i.e.

$$T = T_s(P/P_s)^{(\gamma-1)/\gamma}, \quad \gamma = 1{\cdot}4, \tag{2.3}$$

where P_s and T_s are the pressure and temperature of the air immediately following the passage of the shock front. The *deviation* in temperature from the adiabatic relation (2.3) due to the heat of condensation associated with ΔX is

$$\Delta T = -(L/C_p)\Delta X, \tag{2.4}$$

where C_p is the specific heat of air at constant pressure ($1{\cdot}01 \times 10^7\,\text{erg g}^{-1}\,^\circ\text{K}^{-1}$). From (2.1) and (2.2) it is easily seen that the neglect of ΔX results in an *error* in the relative humidity $\Delta S/S = 17{\cdot}45\,\Delta T/T + \Delta X/X$. As a result of our numerical computations we find *a posteriori* that ΔX is at worst $0{\cdot}5 \times 10^{-4}$ and hence $\Delta T \simeq 0{\cdot}1\,^\circ\text{K}$ in the densest part of the cloud for an explosion energy of the order of 10 kt (we assume throughout a typical maritime aerosol number density of 100 cm^{-3}). Since X is typically 10^{-2} we find that $\Delta S/S$ is of the order of 1 %. This is small compared with the large change in S, say 30–40 %, in the densest part of the cloud. This justifies the use of existing dry-air shock flow results. In § 4, we discuss the breakdown of this approximation for larger explosion energies. We note in passing that in the region of cloud formation the heating of the air due to the absorption of radiation from the fireball at the centre

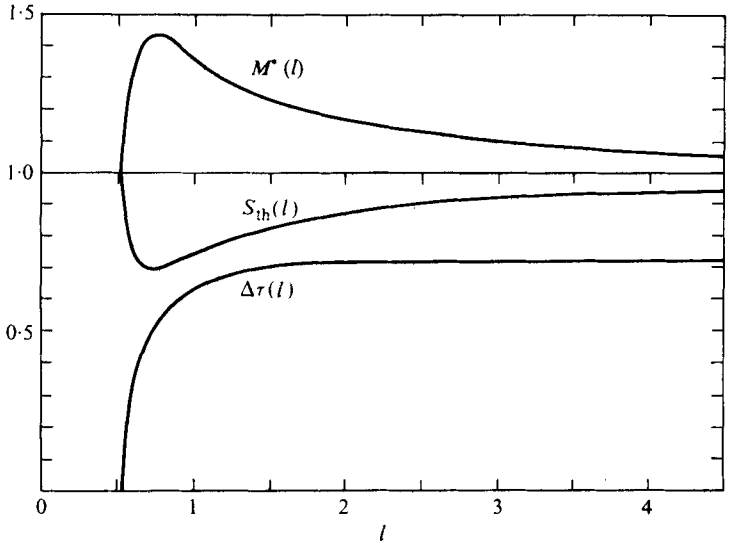

FIGURE 2. Relative humidity threshold for cloud formation $S_{th}(l)$, *vs.* $M^*(l) = [S_{th}(l)]^{-1}$ and the pulse duration $\Delta\tau(l)$ for $M > 1{\cdot}0$ *vs.* dynamic length l.

of the explosion (see Glasstone 1962, p. 49) is much less than the ΔT calculated here.

Thus decoupling shock flow from cloud formation allows us to proceed as follows. Using $\Delta X \ll X$ we have upon direct substitution of (2.2) into (2.1) and use of the ideal-gas law

$$S(r,z,t) = S_0(z)\,(P/P_0)\,[\overline{p}(T_0)/\overline{p}(T)] = S_0(z)\,M(r,t), \tag{2.5}$$

where

$$M = (P/P_0)\exp\left[17{\cdot}45\left(\frac{300}{T_0}\right)\left(\frac{P_0\rho}{P\rho_0}-1\right)\right]. \tag{2.6}$$

P_0, T_0, ρ_0 and S_0 are respectively the ambient pressure, temperature, density and relative humidity of the parcel in question. M depends on P/P_0 and ρ/ρ_0. These ratios are functions of $l = r/r_0$ and $\tau = t/t_0$ only. Here r_0 and t_0 are the dynamic length and dynamic time of the explosion (Sedov 1959, pp. 238–251):

$$r_0 \equiv (E/P_0)^{\frac{1}{3}}, \quad t_0 \equiv E^{\frac{1}{2}}P_0^{-\frac{5}{6}}\rho_0^{\frac{1}{2}}, \tag{2.7}$$

where E is the hydrodynamic energy of the explosion. (For example, at sea level under standard conditions $r_0 \simeq 0{\cdot}8$ km and $t_0 \simeq 2{\cdot}8$ s for $E = 10$ kt.) Figure 1 gives the universal function $M(\tau, l)$ *vs.* τ for various l values ($T_0 = 288{\cdot}15$ °K is used). These curves are based on the numerical treatments of shock profiles due to Needham *et al.* (1973). Their work is in apparent agreement with that reported in Bethe *et al.* (1949) and Sedov (1959). We refer the reader unfamiliar with the theory of shock waves from explosions to the thorough treatment in the latter reference.

As we shall see below, significant cloud formation, i.e. large droplet growth, results only when the relative humidity in a parcel at l is driven to supersaturation $S > 1{\cdot}0$. Thus, from (2.5) there is an energy-independent threshold $S_{th}(l)$ of the ambient humidity for cloud formation at each l given by $M^*(l)^{-1} = \{\max[M(\tau, l)]\}^{-1}$. Figure 2 plots $S_{th}(l)$ *vs.* l [$\Delta\tau(l)$ is defined after (4.2)]. We find from figure 1 that, regardless of S_0, cloud formation can begin only after a time $\tau \simeq 0{\cdot}35$ and outside a radius $l \simeq 0{\cdot}6$.

We emphasize here that cloud formation first begins during a period when neither strong shock (self-similar) theory nor weak shock (asymptotic) theory is valid. From $\tau \sim 0{\cdot}03$ to $\tau \sim 1$, a numerical treatment of the shock hydrodynamics is required. We note in passing that in the region of cloud formation spatial motion of the parcel due to shock winds is generally small and of no interest to the problem. A striking feature apparent from figure 2 is that if the ambient humidity is nowhere greater than 70% then no Wilson Cloud of significance can form.

3. Droplet growth kinetics

From Mason (1971), the equation of growth for a salt-solution droplet, the principal constituent of maritime aerosols, is

$$\bar{r}(d\bar{r}/dt) = [S(t) - S_{\mathrm{eq}}(\bar{r}, m)]/Y(T), \tag{3.1}$$

where S is the shock-driven relative humidity in the air parcel containing the droplet as discussed above, $S_{\mathrm{eq}}(\bar{r}, m)$ is the equilibrium relative humidity for a droplet with radius $\bar{r}$ and salt mass m, and $Y(T)$ is a weakly temperature-dependent coefficient determined by the heat and water-vapour diffusion rates in air. In cgs units

$$S_{\mathrm{eq}}(\bar{r}, m) = \exp(2\sigma\epsilon/\rho_L R_d T\bar{r}) - 3imM/4\pi\rho_L W\bar{r}^3, \tag{3.2}$$

$$Y(T) = (L\rho_L/KT)[L\epsilon/(R_d T) - 1] + \rho_L R_d T/[D\epsilon P_S(T)],$$

$$Y(300\ ^\circ\mathrm{K}) = 7{\cdot}26 \times 10^5\ \mathrm{s/cm^2}, \tag{3.3}$$

where the quantities not given previously are defined as

ρ_L = density of liquid water = 1 g cm^{-3},
σ = surface tension of water = 72 dyne cm^{-1},
K = thermal conductivity of air = $2{\cdot}5 \times 10^3$ erg cm^{-1} s^{-1},
D = water-vapour diffusivity in air = 2×10^{-1} cm^2 s^{-1},
i = Van Hoff's constant = 2·7,
M = molecular weight of water = 18,
W = molecular weight of salt = 58.

It is assumed in deriving (3.1) that water vapour and heat are transported through steady profiles around the droplet. This is justified since, as a result of our numerical calculations, we find *a posteriori* that the characteristic transport time $\tau_D = r_D^2/D$ is at worst only 0·1 % of the characteristic growth and evaporation time regardless of the explosion energy. Here r_D is the radius containing the water vapour required to form a droplet of radius $\bar{r}$, i.e. $(\bar{r}_D = \rho_L/X\rho_0)^{\frac{2}{3}}\bar{r}^2 \simeq 2000\,\bar{r}^2$, and D is the diffusivity.

We now give a numerical illustration of the droplet growth and evaporation cycle. Using the function M shown in figure 1 to find $S(T)$, we have numerically integrated the growth (3.1) for five typical droplet species of salt mass m_i and relative number density n_i (see Mason 1971, p. 60) contained in a typical shocked air parcel. For this case $S_0 = 0{\cdot}89$, $E \simeq 14$ kt and $r \simeq 0{\cdot}9$ km, or $l \simeq 1$. As will be apparent below, $l \sim 1$ corresponds to the region of maximum droplet growth. In figure 3, the relative humidity S seen by the droplets is plotted versus their radii from their entrance into

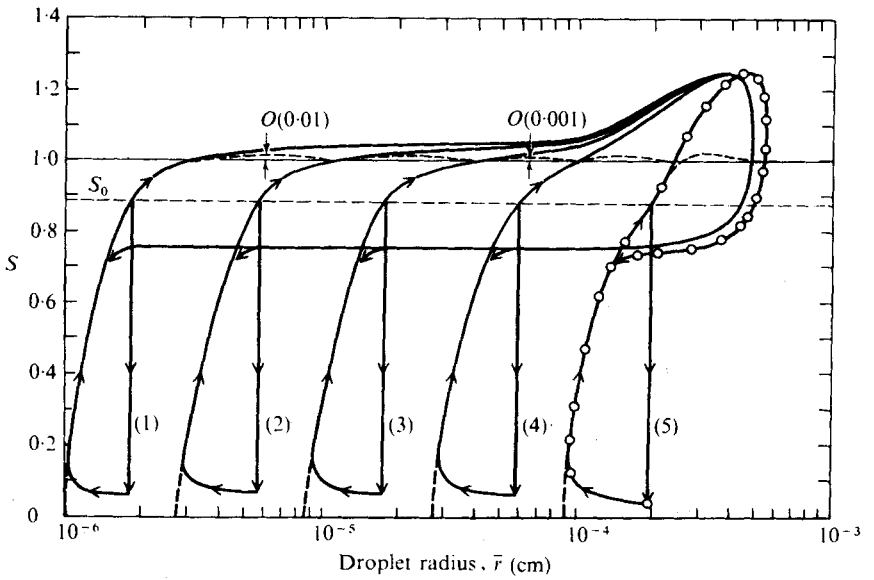

FIGURE 3. Droplet growth and evaporation curves in the relative humidity (S), droplet radius ($\bar{r}$) plane. ---, $S_{eq}(\bar{r}, m)$; ○, time-step fiducials. Salt mass (g): $m_1 = 0{\cdot}488 \times 10^{-17}$, $m_2 = 0{\cdot}117 \times 10^{15}$, $m_3 = 0{\cdot}354 \times 10^{-14}$, $m_4 = 0{\cdot}105 \times 10^{-13}$, $m_5 = 0{\cdot}34 \times 10^{-12}$. Relative number: $n_1 = 0{\cdot}051$, $n_2 = 0{\cdot}210$, $n_3 = 0{\cdot}443$, $n_4 = 0{\cdot}277$, $n_5 = 0{\cdot}018$.

the shock until their evaporation behind the advancing clouds. The $S_{eq}(r, m_i)$ curves are also shown. Upon entering the shock wave a droplet quickly evaporates after a sudden drop in S, then its nucleus returns to its equilibrium curve. It remains there until S is driven beyond supersaturation, at which point rapid droplet growth begins. Each species tagged by its initial mass is found to grow to nearly the same maximum radius. This feature, which we shall call universal growth, is particularly striking in Wilson Cloud growth in that the droplet size at maximum growth is independent of the ambient aerosol spectrum.

Universal growth may be understood by noting that, for each droplet species, once S rises above unity, where significant growth results, $S_{eq}(\bar{r}, m)$ for the resulting $\bar{r}$ is very nearly equal to unity and may be replaced by unity in (3.1). This allows the growth equation to be rewritten in terms of scaled variables and the universal function $M(\tau, l)$ driving the relative humidity. We have then, independent of the species, i.e. independent of m,

$$d[\tfrac{1}{2}R^2(\tau, l)]/d\tau \simeq [S_0(z)\, M(\tau, l) - 1], \tag{3.4}$$

where

$$\bar{r}^2(t, r, m) = R^2(\tau, l)\, t_0\, Y^{-1}. \tag{3.5}$$

Y is gearly constant over the course of growth and evaporation and we use $Y(300)$ as given above. At a given l, cloud formation begins and maximum growth is obtained at the times for which $M(\tau, l) = S_0^{-1}$. We denote these times as $\tau_1^*(l)$ and $\tau_2^*(l)$, respectively. They may be easily read from figure 1. Since droplets typically attain radii significantly larger than their ambient radii, a suitable initial condition for (3.4) is

$$R^2[\tau_1^*(l), l] \simeq 0, \tag{3.6}$$

independent of the species. No new length scale is introduced thereby and the solution to (3.4) and (3.6) is therefore universal.

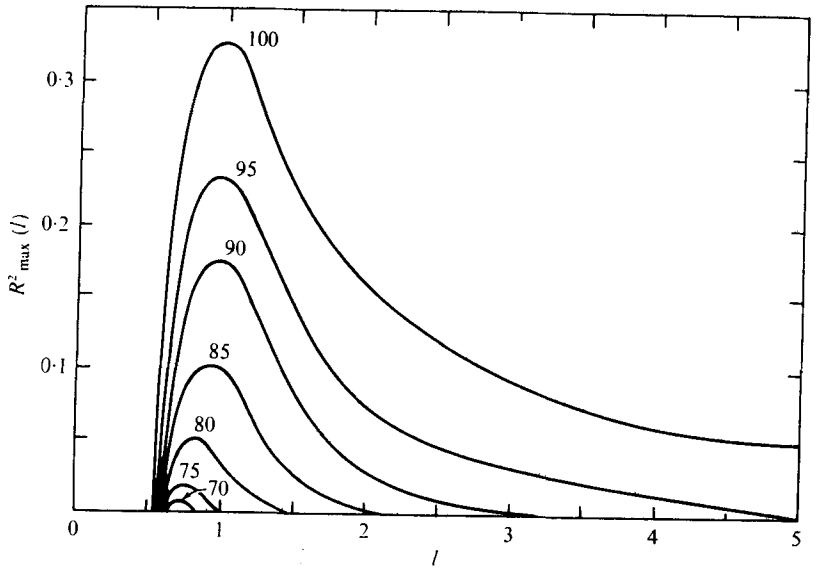

FIGURE 4. Square of the universal maximum droplet radius $R^2_{max}(l)$ *vs.* dynamic length l for various ambient relative humidities.

To clarify the meaning of universal scaled droplet growth [(3.4)–(3.6)] note that this implies the following: if at a distance r and time t from an explosion of energy E the droplet radius in the Wilson Cloud is $\bar{r}$, then for an explosion energy E', $\bar{r}' = r(E'/E)^{\frac{1}{3}}$ at $r' = r(E'/E)^{\frac{1}{3}}$ and $t' = t(E'/E)^{\frac{1}{3}}$ assuming that the same ambient humidity prevails. Furthermore, the approximate cloud droplet size can be calculated entirely without regard to the ambient aerosol spectrum.

4. Results of scaling and universal droplet growth

We present here scaled formulae for maximum droplet size as well as location contours of cloud formation and evaporation. For each l value, i.e. each distance from the explosion centre, we may approximate that portion of the function M greater than unity as a parabola:

$$M(\tau, l) \simeq [M^*(l) - 1](1 - y^2) + 1, \tag{4.1}$$

where $M^*(l)$ is the maximum of M for the given l (see figure 2) and

$$y = [(\tau - \tau_2) + \tfrac{1}{2}\Delta\tau]/\tfrac{1}{2}\Delta\tau, \tag{4.2}$$

where $\Delta\tau(l) = \tau_2(l) - \tau_1(l)$ and τ_1 and τ_2 are the times at which M passes through unity.

Integrating the scaled droplet growth (3.4), subject to the universal initial condition (3.6), over the time interval when $S_0 M \geqslant 1{\cdot}0$ (i.e. between $\tau_1^* \geqslant \tau_1$ and $\tau_2^* \leqslant \tau_2$), we find using (4.1) that

$$R^2_{max}(l) = R^2[\tau_2^*(l), l] = \tfrac{4}{3}\Delta\tau(l)\left\{\left[\frac{S_0}{S_{th}(l)}\right] - 1\right\}\left\{\frac{1 - [S_{th}(l)/S_0]}{1 - S_{th}(l)}\right\}^{\frac{1}{2}}. \tag{4.3}$$

$\Delta\tau(l)$ is plotted in figure 2 along with $S_{th}(l)$ while $R^2_{max}(l)$ is plotted in figure 4 for various ambient humidities.

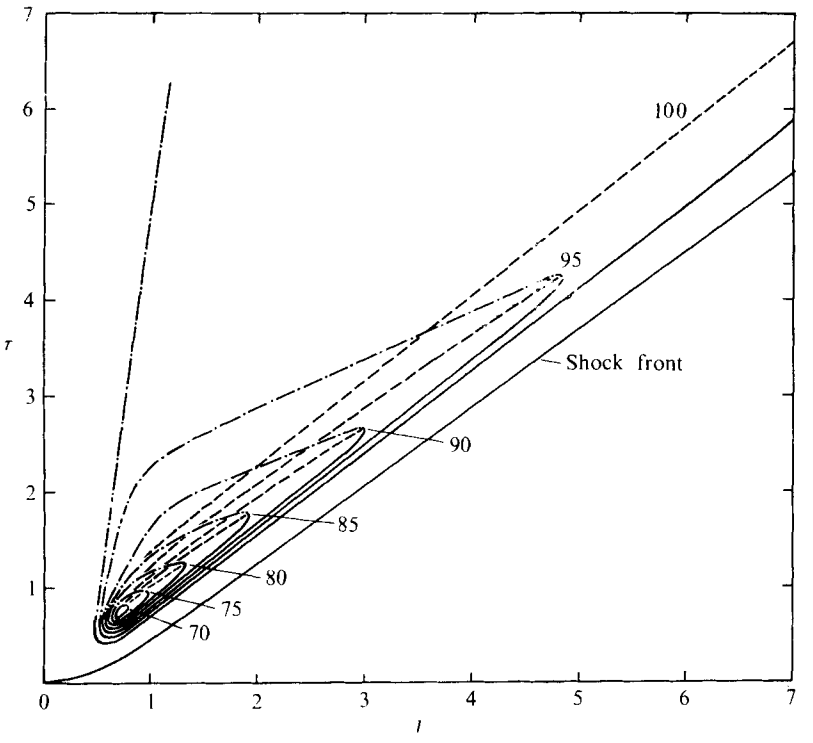

FIGURE 5. Contours of cloud formation time τ_1^*, time of maximum growth τ_2^* and evaporation time τ_3^* *vs.* dynamic length l for various ambient relative humidities. ——, τ_1^*; – – –, τ_2^*; —·—, τ_3^*.

By using the exact M functions to integrate (3.4) beyond $\tau_2^*(l)$ to evaporation, where R^2 returns to zero, we obtain the evaporation time $\tau_3^*(l)$. Figure 5 gives contours of the times of cloud formation $\tau_1^*(l)$, maximum growth $\tau_2^*(l)$ and evaporation $\tau_3^*(l)$ for various ambient relative humidities ranging from 70 to 100 %. Note that, as the relative humidity approaches 100 %, the cloud once formed at a given location l requires an increasingly longer time to evaporate. (This results from the fact that, according to (3.1), the rate of evaporation is proportional to $S_{eq} - S$, which is roughly $1 - S_0$ over much of the evaporation phase.) The contours may be read at constant τ to find the location of the outside and inside of the cloud, as well as the l value of maximum growth. Figure 4 and equation (3.5) may then be used to find the maximum droplet radius.

The scaling laws may be used to find the limits of validity for the approach taken here. We have noted in § 2 that, for E of the order of 10 kt and with water condensation neglected, ΔX results in errors in S of the order of 1 %. Since droplet radii scale as $E^{\frac{1}{3}}$, ΔX scales as $E^{\frac{1}{3}}$. Thus for E of the order of 100 kt, the error in S would be of order 3 %, which is unacceptably large compared with a typical supersaturation in the densest part of the cloud. Thus, for accurate results larger energies require a treatment which couples cloud formation to shock hydrodynamics, the simple scaling laws presented here being inadequate. Also, we remind the reader that ΔX is directly proportional to the number density of an aerosol. If it is larger than the 100 cm^{-3} assumed here, then the upper limit of validity must be rescaled downwards.

The universal droplet growth equations will also show breakdown for very low explosion energies such that the length scale introduced by the ambient droplet sizes becomes important. This is the case if the typical values of $R^2_{\max}(l)$ given by (4.2) or figure 4 are not considerably larger than $R_0^2 \equiv \bar{r}_0^2 t_0^{-1} Y$, where $\bar{r}_0(\overline{m})$ is the equilibrium radius of a representative droplet species at 100 % relative humidity. Let us consider a median salt grain such as (3) in figure 3, which has $\bar{r}_0 = 4{\cdot}5 \times 10^{-5}$ cm. For $E = 10$ kt, this corresponds to $R_0^2 \sim 0{\cdot}5 \times 10^{-3}$. This is well above the typical values of $R^2_{\max}$, which, in turn, are conservatively of the order of 0·01. However, since R_0^2 scales like $E^{-\frac{1}{3}}$, we expect our treatment to break down for E less than about 10^{-3} kt.

The author wishes to thank Dr O. P. Manley and Dr R. C. Englade of Visidyne, Inc., for many useful discussions on the topic of Wilson Cloud formation. This research was sponsored by the Defense Nuclear Agency under Subtask S99QAX H1004, Work Unit 11, entitled OPTIR Code and Aircraft Measurements.

REFERENCES

BETHE, H. A. *et al.* 1949 Blast wave. *Los Alamos Sci. Lab. Rep.* LA-2000.

GLASSTONE, S. 1962 *Effects of Nuclear Weapons*, pp. 47–49. U.S. Dept. Defense.

MASON, B. J. 1971 *The Physics of Clouds*, pp. 122–125. Oxford: Clarendon Press.

NEEDHAM, C. E. *et al.* 1973 Nuclear blast standard (1 kt). *Air Force Weapons Lab. Tech. Rep.* AFWL-TR-73-55.

SEDOV, L. I. 1959 *Similarity and Dimensional Methods in Mechanics*, pp. 238–251. Academic Press.